scientific reports

Check for updates

OPEN

From Himba indigenous knowledge to engineered Fe_2O_3 UV-blocking green nanocosmetics

D. Havenga[1,2,3]✉, R. Akoba[1,2], L. Menzi[1,2], S. Azizi[1,2], J. Sackey[1,2], N. Swanepoel[3], A. Gibaud[1,2,4] & M. Maaza[1,2]✉

This contribution reports on the physical properties of the natural Namibian red Ochre used by the Himba Community in a form of a formulation, so called Otjize as a skin protective and beauty cream. The morphological and crystallographic studies of this red ochre validated its nano-scaled dominating phase of rhombohedral α-Fe_2O_3 nanocrystals with an additional hydrolized oxide component in a form of γ-FeOOH. The optical investigations showed that such a red ochre exhibits an exceptional UV filtration and a significant IR reflectivity substantiating its effectiveness as an effective UV-blocking & solar heat IR reflector in support of the low skin cancer rate within the Namibian Himba community. In addition, such nanocrystals exhibited a non-negligible antibacterial response against E. Coli & S. Aurus. This study seems confirming the effectiveness of the indigenous Otjize as an effective skin UV protection cream with a sound antimicrobial efficacy against e-Coli & S-Aurus.

In addition to the recently discovered Zeta-Fe_2O_3 structure[1], Iron (III) oxide represents one of the most rich and multifunctional oxide families[2]. It has four standard principal polymorphs, hematite (α-Fe_2O_3), maghemite (γ-Fe_2O_3), β-Fe_2O_3 and ε-Fe_2O_3; iron (III) oxy-hydroxide also has four polymorphs known as goethite (α-FeOOH), akaganeite (β-FeOOH), lepidocrocite (γ-FeOOH) and feroxyhyte (δ-FeOOH)[2]. Of a special interest, α-Fe2O3 is a prominent n-type semiconductor with an interesting bandgap Eg = 2.1 eV, conjugated to an excellent chemical stability and low toxicity under ambient conditions. Among these oxides, α-FeOOH and α-Fe2O3 have been commonly investigated for magnetic devices, catalysts, gas sensors and photoelectrodes applications[3–10] in addition to pigment production. However, it is worth noting that this latter pigment aspect has been identified as early as the birth of humanity.

Indeed, early human used several marine resources and pigments to express artistically on their natural surroundings & believes ranging from prehistoric, ochre-pigmented images on cave walls to paintings on canvasses in addition to their symbolic behaviors. Its usage in symbolic behavior was found to date164,000 years ago, far earlier than previously documented[11].

More precisely, the earliest evidence of the ochre pigment's usage by ancient humans dates to the Paleolithic, about 285,000 years ago, at a Homo erectus site called GnJh-03 in Kenya. In this location, archaeologists discovered about 70 pieces of ochre weighing about 5 kg[12].

Early Homo-sapiens also illustrated extensively with ochre pigment. At Blombos Cave, in South Africa, archaeologists discovered an abalone shell containing finely ground ochre, charcoal as well as fat that may have made up a likely painting kit dating to about 100,000 years ago. The earliest human-made drawing is a red hashtag on small rock flake that dates to about 73,000 years ago, also at Blombos and Klein Kliphuis Caves in South Africa. In addition, about 266,000 years ago, early hominins at a site called Twin Rivers in Zambia collected a type of hematite ochre that has significantly reflective metallic flakes in it making it glittering[13–15].

As highlighted previously, while Ochre was used as an effective artistic & behavioral pigment in various locations within the African continent, the Himba ethnic group specifically, has genuinely extended its usage towards cosmetic & skin-protection applications (Fig. 1a). With the Nama & the Herero communities, the Himba society is an additional indigenous social group in Namibia. Living in the northern part within the Kunene region, they are hunter-gatherers, semi-nomadics & pastoralists. Exposed to harsh atmospheric conditions in general

[1]College of Graduate Studies, UNESCO-UNISA Africa Chair in Nanosciences-Nanotechnology, Muckleneuk Ridge, PO Box 392, Pretoria, South Africa. [2]Nanosciences African Network (NANOAFNET), iThemba LABS-National Research Foundation, 1 Old Faure Road, Somerset West, Western Cape 7129, PO Box 722, Johannesburg, South Africa. [3]Department of Anthropology & Archaeology, College Human Sciences University of South Africa, PO Box 392, Pretoria, South Africa. [4]Physics Dept, University of Le Mans, Le Maine, France. ✉email: havengads@gmail.com; Maazam@unisa.ac.za

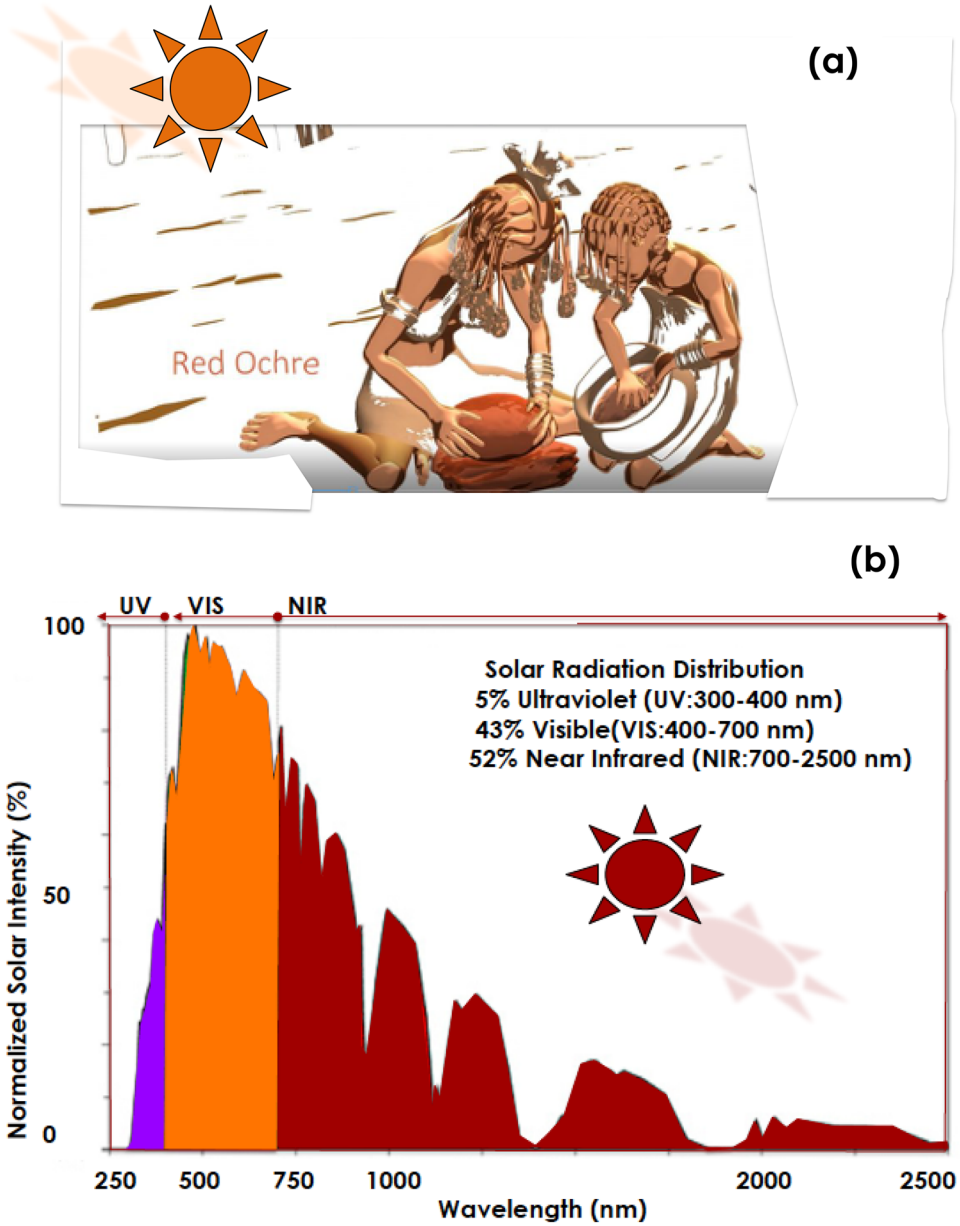

Figure 1. (**a**) Traditional preparation of the Red Ochre pigment by the Himba community, (**b**) Solar spectral distribution in the north of Namibia to which the Himba group community is exposed.

and daily solar radiations especially where the Direct Normal irradiation is among the highest globally. In the quasi-absence of clouds, they are exposed through out the year to the standard 5% UV (300–400 nm), 43% VIS (400–700 nm) and 52% NIR-FIR (700–2500 nm) solar radiations (Fig. 1b). Accustomed to a semi-arid climate, the Himba women are famous for covering their skin & hairs with the so called Otjize paste[16]; a cosmetic mixture of goat-butterfat and ochre pigment.

Otjize cleanses the skin over long periods due to water scarcity and considered as an effective protection from the hot and dry climate, as well as from insect bites. It gives Himba people's skin and hair plaits a distinctive texture, style, and orange or red tinge, and is often perfumed with the aromatic resin of the indigenous omuzumba shrub (*Commiphora* multijuga)[17]. From anthropological viewpoint, Otjize is considered foremost a highly desirable aesthetic beauty cosmetic, symbolizing earth's rich red colour and blood, the essence of life, and is consistent with the Himba ideal of beauty (Fig. 1a).

To validate the optical filtering & selectivity as well as the health skin protection of the Ochre pigment used in the Himba Otjize, this contribution reports on its physical properties with a special focus on their optical selectivity in the UV–VIS spectral solar range and their antibacterial efficacy. If so, this would be the originality & novelty of this contribution.

Experiments, results & discussion

For this study, typical Himba Ochre samples from the Kunene region of Namibia were collected from a Himba settlement. They were used without any further physical–chemical treatment. The samples were investigated by High Resolution Scanning Electron microscopy (HRSEM) for their morphological constituency, High Resolution Transmission Electron Microscopy (HRTEM) for the shape & atomic ordering of the elementary crystals if any, Energy Dispersive Spectrometry (EDS) for elemental analysis in addition to room temperature X-Rays Diffraction (XRD) for their crystallographic structure.

These studies were complemented with a full range of optical investigations (Photoluminescence, Infrared & UV–VIS spectroscopies). The antibacterial activity was carried out on 2 standard bacterial species: E-coli & Staphylococus Aurus.

Morphology & crystallographic investigations. Figure 2a reports the HRSEM of the Himba ochre. As one could notice, it consists of agglomerated lamellar nanoplatelets. Their longitudinal & basal dimensions are relatively wide spread in terms of dimension. The average basal dimension is estimated within the range of 17–31 nm while the longitudinal average dimension is above 100 nm. Figure 2b reports an HRTEM of the Himba Ochre after sonication. The lamellar nano-platelets seem consisting of nanoscale relatively crystalline grains with preferred crystalline orientation and a platelets type morphology. The major observed atomic ordering correponds to an inter-reticular distance of 5.03 Å in agreement with the (104) atomic orientation of pure single phase hematite α-Fe_2O_3. Figure 2c displays the size distribution of the nanoparticles obtained by standard light scattering. The corresponding profile indicates a relatively polydisperse nanosystem with an average size of $<\phi> = 148.3$ nm. In this analysis, the nano-platelets were approximated as spheroids with a diameter ϕ. This latter parameter could be almost be the equivalent of the size of the nanoplatelets.

Figure 2d reports the XRD diffraction pattern of the Ochre sample within the angular range 2θ of 22.5–65 Deg. One can distinguish 2families of diffraction Bragg peaks. The first one is identified & indexed as (012), (104), (110), (113), (024), (116), (018), (214) and (030) of the rhombohedral single phase α -hematite α -Fe_2O_3. The second family set is characterized by the following diffraction Brag peak. Namely (120), (021), (111), (121), (221), (151). This later set corresponds to γ-FeOOH. It should be noted that (104) diffraction Bragg peak is one of the most intense peak, in agreement with the atomic ordering of the nanocrystals with a preferred lattice atomic ordering of $d_{hkl} = 5.04$ Å observed in the previous HRTEM studies of Fig. 2b. In a pre-conclusion, the Himba Ochre sample consists of hematite α-Fe_2O_3 mainly with an amount of a hydrolized form in a form of γ-FeOOH. In view of investigating the thermal stability of such a nano-system, Differential Scanning Calorimetry (DSC) studies under standard air were conducted within the thermal range of 25–650 °C. Figure 2e reports the corresponding DSC profile. This latter exhibits 3 major zones with an exothermic and an endothermic peaks with the first zones. Zone 1 is likely to be related to the melting/evaporation of H_2O molecules adsorbed onto the sample surface. Zone 2 corresponds likely to a phase transformation of FeOOH to α -Fe_2O_3[18–24].

Elemental investigations. Figure 3a depicts their corresponding elemental EDS spectrum. There are 4 major Fe peaks located at various channels with the O peak as the most intense. The C peak originates from the Carbon coating used to avoid surface charging effect during the HRSEM investigations. Likewise, one can distinguish the presence of several contaminants including Mg, Al, Si, K, Ca & Ba. Figure 3b reports their corresponding 2D scans showing that they are relatively homogeneously distributed within the Ochre sample yet at low concentrations. Their qualitatively values are significantly at low levels i.e. impurities level relatively to Fe & O. The relative atomic ratio of O/Fe is about 1.62 suggesting that the the Himba Ochre is likely hematite Fe_2O_3 (O/Fe = 1.5) rather than magnetite Fe_3O_4(O/Fe = 1.3).

Vibrational spectroscopy investigations. Figure 4a reports the Attenuated Total Reflection (ATR)-Fourier Transform InfraRed (FTIR) spectrum of the Himba Ochre within the 400–4000 cm^{-1} spectral range. One can notice the relatively sharp mode at 451 cm^{-1} & the convoluted peaks at 545 & 602 cm^{-1} which are characteristic of the Fe–O vibrational modes. The various absorption modes from 801–1688 cm^{-1} are assigned to C=O, C–O–C stretching modes related to adsorbed CO_2 molecules on the surface of the α-Fe_2O_3 crystals. In addition to the 2 low intensity vibrational modes of 1794 & 2347 cm^{-1} assigned to H_2O & CH_2 respectively, there is a broad band stretching from 2750–3700 cm^{-1} which may rise from various vibrational modes of H_2O molecules. The latter molecules are likely due to atmospheric water molecules adsorbed on the surface of the α-Fe_2O_3 nano-crystals or those of the γ-FeOOH.

Defects & luminescence investigations. From luminescence viewpoint in defects free α -Fe_2O_3, luminescence emissions would originates from the valence band of the Fe (3d) and O (2p) states, to the conduction band dominated by Fe (4 s) states. Because the local configuration of the d-band, α-Fe_2O_3 does not exhibit photoluminescence emission in its bulk form[25]. Figure 4b reports the luminescence spectrum at room temperature of the Otjize ochre sample under an excitation of 270 nm. It shows a relatively intense emission with a shoulder. More precisely, The simulation of the emission profile consists of 1 broad & 2 sharp emissions centered at 485, 479 and 593 nm respectively. The origin of these luminescence emissions could be due to two major factors: (i) the Oxygen surface atomic coordination as per the Pauling & Hendrick's model for α -Fe_2O_3[26] (ii) An increase in the F-O bonding separation inducing an enhancement in the magnetic coupling between Fe^{3+} ions neighbours as reported by Han et al.[27] and Blake et al.[28],, (iii)surface defects which may arise from deep traps caused by Fe vacancies[28].

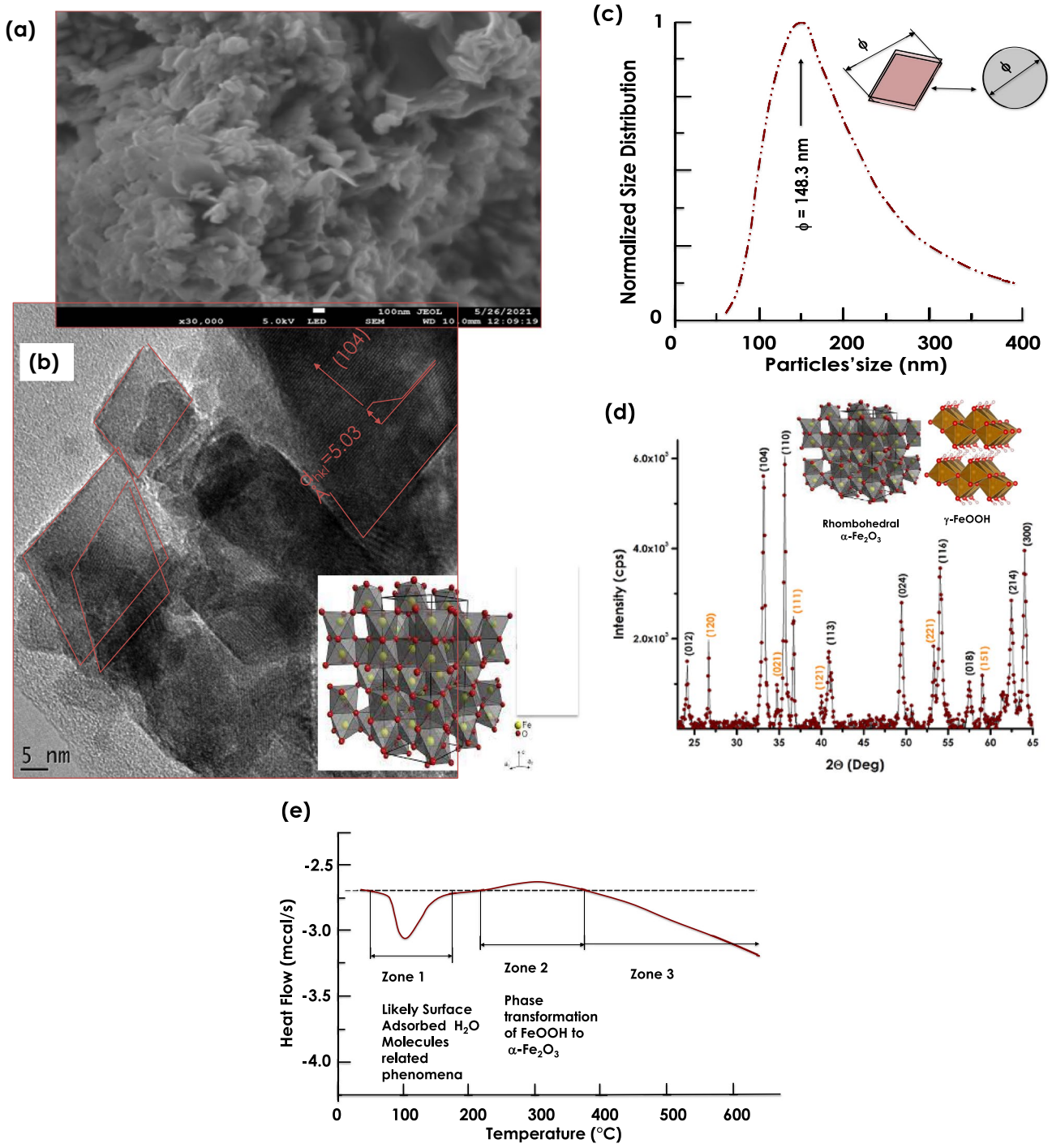

Figure 2. (**a**) High Resolution SEM image of the Red Ochre pigment, (**b**) its High Resolution TEM observation of the crystalline rhombohedral nanoplatelets like-particles, (**c**) their Size distribution, (**d**) its corresponding room temperature X-Ray diffraction pattern, and (**e**) their differential scanning calorimetry within the temperature range of 25–600 °C.

Optical investigations & UV selectivity. In terms of optical absorbance, standard hematite α-Fe_2O_3 exhibits several absorbance bands centered at about 347 nm, 543 nm assigned to metal charge transfer direct transitions and to the double excitation processes $^6A1(6\,s) + {}^6A_1(6\,s)$ to $^4T_1(^4G) + {}^4T_1(^4G)$ respectively[29]. Those in the range of 478–550 nm are caused by $^6A_1(6\,s)$ to ^4E, $^4A_1(^4G)$ ligand field transitions[30]. In addition to these various absorbance bands, there is a strong absorbance at 543 nm which at the origin of the red color of hematite. Figure 4c reports the Reflectance of the Otjize ochre sample in the spectral range of 190–2500 nm. As one can notice, there is a sharp spectral cut-off at about 570 nm. The reflectance is minimal below such a cut-off; < 3%. Because of the opacity of the sample, the spectral range in the UV & part of the VIS is fully absorbed by the Otjize

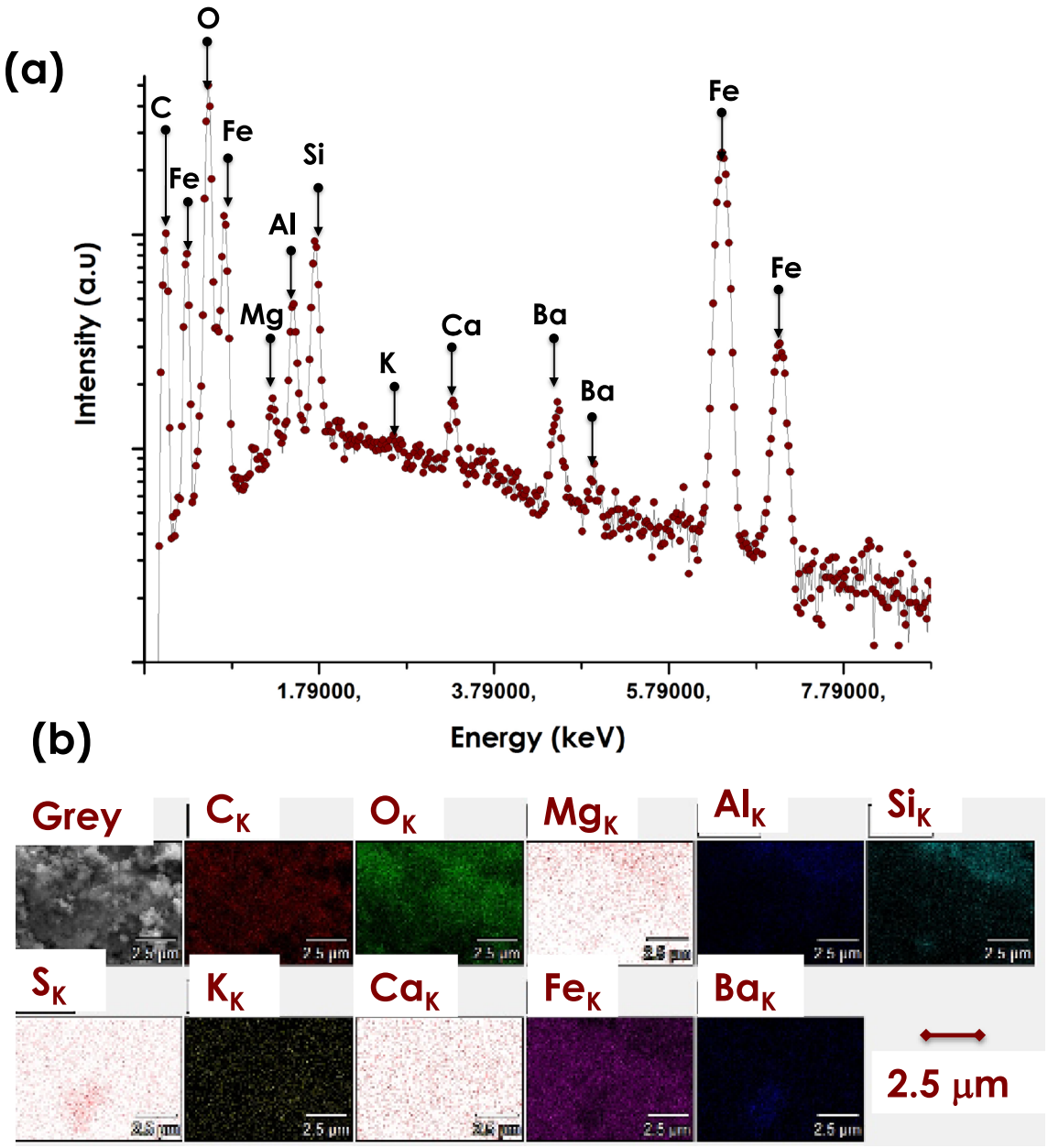

Figure 3. (**a**) EDS elemental spectrum of the Red Ochre pigment & (**b**) its corresponding 2-D disctribution scan of the various detected elements.

ochre sample in the measured spectral range of 190–570 nm. Hence, it can be concluded that the Otjize ochre sample is an exceptional UVA & UVB selective filter & hence an effective shield against solar UV radiations induced skin cancer. Following a dip in the reflectance centered at 855 nm, there is a plateau-like with an average of 53.6% suggesting that the Otjize ochre coating minimizes the skin overheating by reflecting-back at least half of the solar heat in the IR region. While the dip centered at 855 nm is due to of $^{6}A_{1}(6\ s)$ to $^{4}T_{1}(^{4}G)$ ligand field transition[31], the one at about 1950 nm corresponds to a H_2O absorption window. This latter absorption is likely to be caused by atmospheric H_2O molecules adsorbed on the α-Fe_2O_3 Otjize ochre sample. One should mention that this optical cut-off behavior of hematite which makes it of a special interest in solar water photo-splitting applications[7,8,32–34].

Antibacterial studies. Relatively to the standard nano-TiO_2 & nano ZnO possessing cut-off wavelengths at the UV-Bleu spectral range at the vicinity of 380 & 390 nm respectively, the one of the current Himba Otjize red Ochre is by contrast in the visible range at the vicinity of 570 nm as per (Fig. 4c). Consequentially, the nano-scaled α -Fe_2O_3 of the Himba Otjize red Ochre should exhibit an antibacterial response. Indeed, as reported in Fig. 5a, the antibacterial activity against E-coli & staphylococcus-aurus. More precisely, it reports the inhibition zone against E-coli & staphylococcus-aurus at various Himba Otjize red Ochre α-Fe_2O_3 concentrations;50, 100 & 200 µg/µl. One can notice that there is a crystal clear an antibacterial against both species yet relatively low

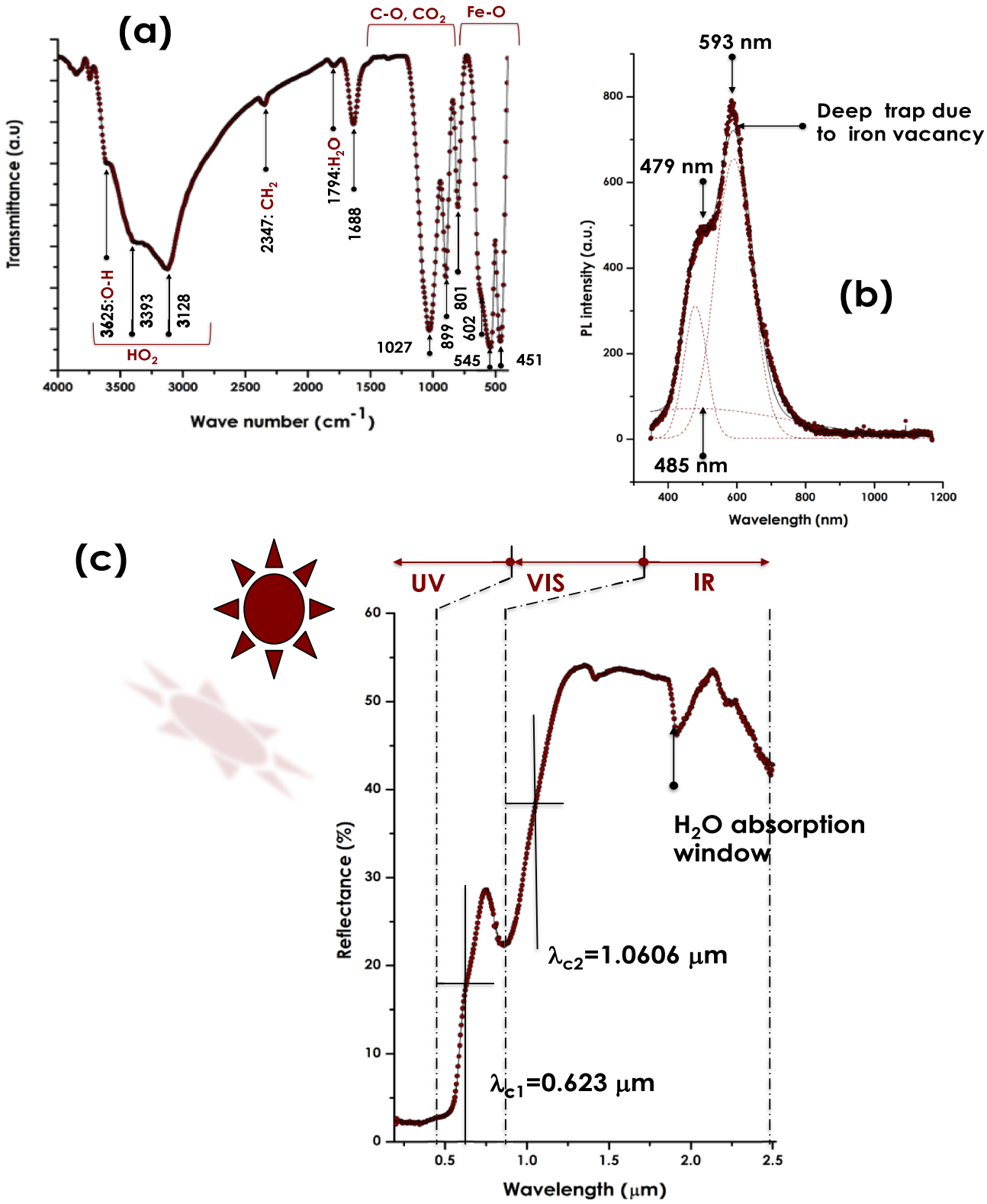

Figure 4. (**a**) ATR-FTIR vibrational modes of the Red Ochre pigment, (**b**) its Photoluminescence emission spectrum under an excitation wavelength $\lambda_{exc} = 270$ nm, and (**c**) its UV–VIS-NIR reflectance in the spectral range of 190–2500 nm.

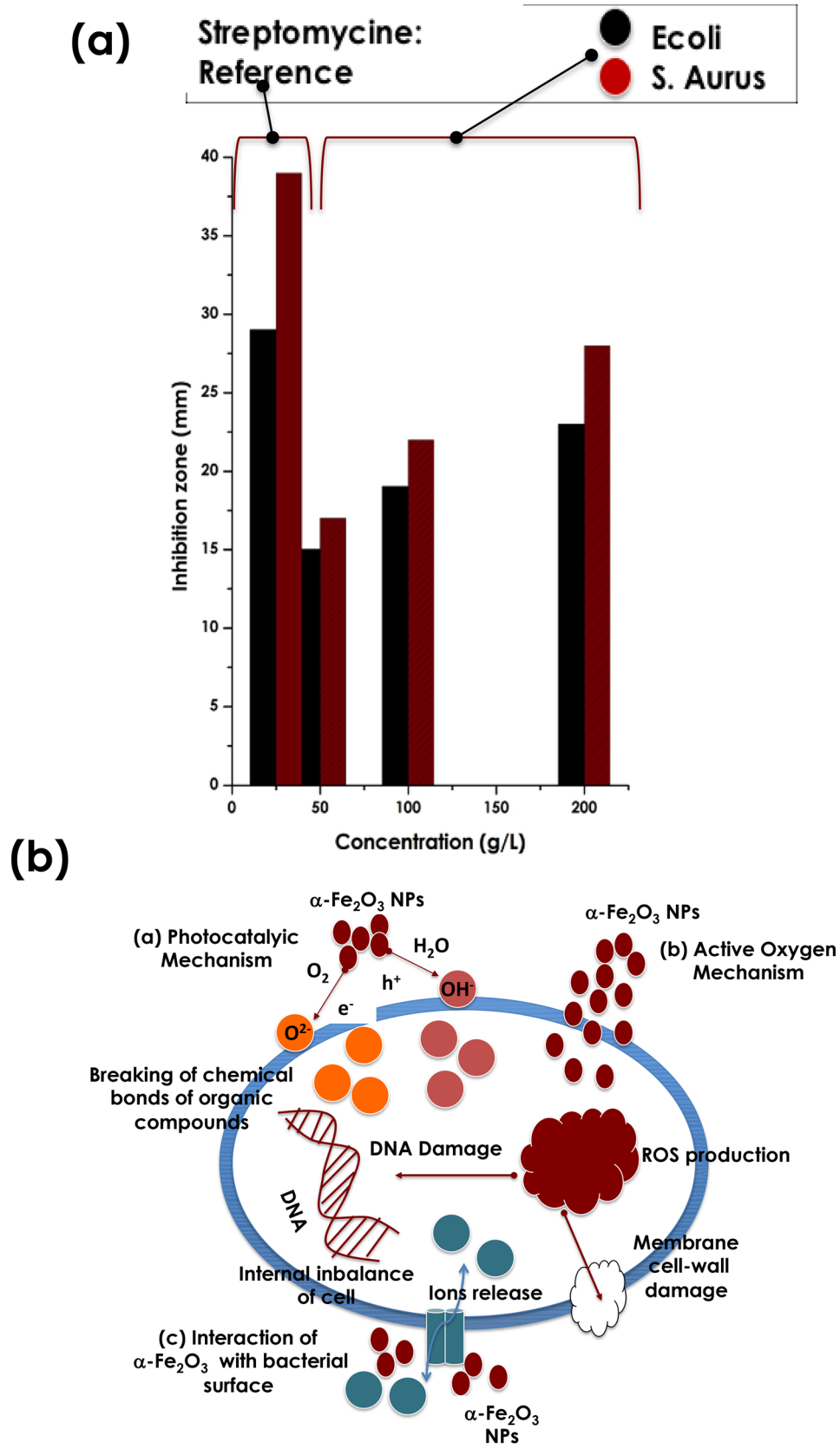

Figure 5. (**a**) Antibacterial response of the Red Ochre pigment against the E-coli & S-Aurus compared to standard reference Streptomycine (**b**), Schematic representation of the 3 potential mechanisms inducing the antibacterial activity of the Ochre.

compared to the standard Streptomycine. However, the efficacy of the Himba Otjize red Ochre α-Fe_2O_3 nanoparticles become effective at higher concentrations. This trend is comparable to those obtained by Rufus et al.[35] on pure hematite bio-synthesized using natural extract of Psidium guajava's leaves as an effective chelating agent.

In terms of the antibacterial activity of the nano-scaled α-Fe_2O_3 of the Himba Otjize red Ochre, one can distinguish 3 potentials mechanisms which are schematically represented in Fig. 5b[36–43];

(i) Photocatalytic mechanism, (ii)Reactive Oxygen Species mechanism & or (iii)Cell surface interaction with the α-Fe_2O_3 nanoparticles mechanism. In the first mechanism, once the the α-Fe_2O_3 nanoparticles are excited with a light energy larger than the bandgap, an e^-–H^+ excitonic pair is created. This e^-–H^+ pair reacts with O_2, hydroxyl groups as well as the adsorbed H_2O molecules to produce sturdy oxidative compounds such as OH^-, O^{2-} and H_2O_2. The H^+ and OH^- are characterized by strong oxidative properties, able to break the chemical bonds of various compounds inducing the degradation of the micro-organisms and therefore antibacterial effectiveness. The second potential mechanism involves Reactive oxygen species. Once diffused in the cell, the nanoscaled α-Fe_2O_3 nanoparticles produce ROS species inducing a severe damage to bacterial membranes and hence bacteriolysis & aggregation of α-Fe_2O_3 nanoparticles within the bacteria leading their death. In the third mechanism, and because of the high surface to volume ratio of the α-Fe_2O_3 nanoparticles, their interaction with the cell surface leads to a significant bacterial membrane damage and the release of ion channels, resulting in internal ionic imbalance of the cells, and eventually death[43,44].

As a major pre-conclusion of this study, it is worth pointing that the effective UV filtration of the red ochre used by the Himba Women could explain the low skin cancer within such a community in Namibia[45].

Conclusion

This study was geared towards the investigation of the bio-physical properties of Red Ochre pigment used by the Himba in their Otjize formulation to protect their skin from solar radiations. It was found that the Red Ochre pigment consisted of nanoscaled particles of mainly α-Fe_2O_3 with γ-FeOOH nanoparticles. Such a Red Ochre pigment exhibited a significant UVA & UVB blocking optical properties hence is an effective skin cancer protection. In addition, it exhibits an effective reflectivity in the IR region hence minimizing solar heat burning of the Himba bodies in the harsh Namibian desertic climate. In addition, it was found that such a red Ochre pigment exhibit additional antibacterial efficacy against E-coli & Staphylococcus Aurus. As a major conclusion of this study, it is worth pointing that the effective UV filtration of the red ochre used by the Himba Women could explain the low skin cancer within such a community in Namibia.

Received: 29 June 2021; Accepted: 18 November 2021
Published online: 10 February 2022

References

1. Tuček, J. *et al.* Zeta-Fe2O3: A new stable polymorph in iron(III) oxide family. *Sci. Rep.* **5**, 1509. https://doi.org/10.1038/srep15091 (2015).
2. Cornell, R. M. & Schwertmann, U. *The Iron Oxides: Structure, Properties, Reactions, Occurrence and Uses* (Wiley-VCH Publishers, 2003).
3. Hanslık, T., Tlaskal, J., Subrt, J. & Zapletal, V. Behaviour of iron (III) oxide hydroxides and iron (III) oxides in concentrated solutions of alkali hydroxides. *Mater. Chem.* **6**, 267–276 (1981).
4. Song, L. & Zhang, S. Formation of α-Fe2O3/FeOOH nanostructures with various morphologies by a hydrothermal route and their photocatalytic properties. *Colloids Surf. A* **348**, 217–220 (2009).
5. Faust, B. C., Hoffmann, M. R. & Bahnemann, D. W. Photocatalytic oxidation of sulfur dioxide in aqueous suspensions of alpha-iron oxide (Fe2O3). *J. Phys. Chem.* **93**, 6371–6381 (1989).
6. Mohapatra, S. K., John, S. E., Banerjee, S. & Misra, M. Water Photooxidation by Smooth and Ultrathin α-Fe2O3 Nanotube Arrays. *Chem. Mater.* **21**, 3048–3055 (2009).
7. Sivula, K., Le Formal, F. & Gratzel, M. Solar water splitting: Progress using hematite (α -Fe2O3) photoelectrodes. *Chemsuschem* **4**, 432–449 (2011).
8. Sivula, K. Photoelectrochemical water splitting with mesoporous hematite prepared by a solution-based colloidal approach. *J. Am. Chem. Soc.* **132**, 7436–7444 (2010).
9. Hermanek, M., Zboril, R., Medrik, I., Pechousek, J. & Gregor, C. Catalytic efficiency of iron(III) oxides in decomposition of hydrogen peroxide: Competition between the surface area and crystallinity of nanoparticles. *J. Am. Chem. Soc.* **129**, 10929–10936 (2007).
10. Mohsan, B. & Shaista, A. Green synthesis of Fe_2O_3 nanoparticles from orange peel extract and a study of its antibacterial activity. *J. Korean Phys. Soc.* **76**(9), 848–854 (2020).
11. Bu, K., Cizdziel, J. V. & Russ, J. The source of iron-oxide pigments used in pecos river style rock paints. *Archaeometry* **55**(6), 1088–1100 (2013).
12. Roebroeks, W. *et al.* Use of red ochre by early Neandertals. *Proc. Natl. Acad. Sci.* **109**(6), 1889–1894 (2012).
13. Henshilwood, C. *et al.* A 100,000-year-old ochre-processing workshop at blombos cave, South Africa. *Science* **334**, 219–222 (2011).
14. Dayet, L., Le Bourdonnec, F. X., Daniel, F., Porraz, G. & Texier, P. J. Ochre Provenance and Procurement Strategies During The Middle Stone Age at Diepkloof Rock Shelter, South Africa. *Archaeometry* **5**, 807–829 (2015).
15. Dayet, L., Texier, P. J., Daniel, F. & Porraz, G. Ochre resources from the Middle Stone Age sequence of Diepkloof Rock Shelter, Western Cape, South Africa. *J. Archaeol. Sci.* **40**(9), 3492–3505 (2013).
16. Bollig, M. & Heinemann, H. Ochre people and heroic herders—visual presentations of the Himba of Namibia's Kaokoland. *Vis. Anthropol.* **15**(3), 267–312 (2002).
17. Crandall, D. P. Himba flora taxonomy and herbal medicines. *Anthropos* **99**(1), 200–207 (2004).
18. Music, S., Krehula, S. & Popovic, S. Thermal decomposition of γ-FeOOH. *Mater. Lett.* **58**, 444–448 (2004).
19. Bashir, M. Solution-processed two-dimensional materials for next-generation photovoltaics. *J. Korean Phys. Soc.* **76**(9), 848–854 (2020).
20. Jiao, H. & Jiao, G. Hydrothermal synthesis and characterization of monodisperse α-Fe2O3 nanoparticles. *Mater. Lett.* **63**, 2725–2727 (2009).
21. Tong, G. *et al.* Rapid preparation of a-FeOOH and a-Fe2O3 nanostructures by microwave heating and their application in electrochemical sensors. *J. Alloys Compd.* **509**, 4320–4326 (2011).

22. Zhang, G.-Y., Xu, Y.-Y., Gao, D.-Z. & Sun, Y.-Q. Materials development and potential applications of transparent ceramics: A review. *J. Alloys Compd.* **509**, 885–890 (2011).
23. Hao, Q. *et al.* Fabrication of LDH nanosheets on β-FeOOH rods and applications for improving the fire safety of epoxy resin. *Solid State Sci.* **12**, 2125–2129 (2010).
24. Diamandescu, L., Mihaila-Tarabasanu, D., Calogero, S., Popescu-Pogrion, N. & Feder, M. Hydrothermal synthesis and characterization of some polycrystalline α-iron oxides. *Solid State Ionics* **101**, 591–596 (1997).
25. Jahagirdar, A. A. *et al.* Structural, EPR, optical and magnetic properties of α-Fe2O3. *Spectrochim. Acta Part A: Mol. Biomol. Spectrosc.* **104**, 512–518 (2013).
26. Pauling, L. & Hendricks, B. "The crystal structures of Hematite & Corundum. *J. Am. Chem. Soc.* **47**(3), 781–790 (1925).
27. Han, Q. *et al.* Low temperature synthesis and photocatalytic activity of rutile TiO2 nanorod superstructures. *J. Phys. Chem. C* **111**, 5034–5038 (2007).
28. Blake, R., Hessevick, R., Zoltai, T. & Finger, L. Refinement of the hematite structure. *Am. Mineral.* **51**, 123–129 (1966).
29. Marusak, L. A., Messier, R. & White, W. B. Electronic spectra of Fe3+ oxides and oxide hydroxides in the near IR to near UV. *J. Phys. Chem. Solids* **41**, 981–984 (1980).
30. Wheeler, D. A., Wang, G., Ling, Y., Li, Y. & Zhang, J. Z. Nanostructured hematite: Synthesis, characterization, charge transfer. *Energy Environ. Sci.* **5**, 6682–6702 (2012).
31. He, Y. P. *et al.* Size and structure effect on optical transitions of iron oxide nanocrystals. *Phys. Rev.* **71**, 125411–125419 (2005).
32. Beermann, N., Vayssieres, L., Lindquist, S. E. & Hagfeldt, A. Photoelectrochemical studies of oriented nanorod thin films of hematite. *J. Electrochem. Soc.* **147**, 2456–2461 (2000).
33. Ozer, N. & Tepehan, F. Optical and electrochemical characteristics of sol–gel deposited iron oxide films. *Sol. Energy Mater. Sol. Cells* **56**, 141–152 (1999).
34. Vayssieres, L. *et al.* Characterization of α-Fe2O3 nano powders synthesized by emulsion precipitation-calcination route and rheological behaviour of α-Fe2O3. *Adv. Mater.* **17**, 2320–2323 (2005).
35. Rufus, A., Sreeju, N. & Philip, D. Synthesis of biogenic hematite (α-Fe_2O3) nanoparticles for antibacterial and nanofluid applications. *RCS Adv.* **6**, 1–26 (2016).
36. Dutta, R. K., Nenavathu, B. P. & Gangishetty, M. K. Studies on antibacterial activity of ZnO nanoparticles by ROS induced lipid peroxidation. *Colloids Surf. B Biointerfac.* **94**, 143–150 (2012).
37. Kuang, H. J., Yang, L. & Xu, H. Y. Antibacterial properties and mechanism of zinc oxide nanoparticles: Research progress. *Chin. J. Pharmacol. Toxicol.* **29**(1), 153–157 (2015).
38. Yamamoto, Y. *et al.* Singlet oxygen from irradiated titanium dioxide and zinc oxide. *Methods Enzymol.* **319**, 29–37 (2000).
39. Chu, L. C., Zhou, Z. W., Duan, X. F. & Tang, L. L. Materials development and potential applications of transparent oxides. *Mater. Rev.* **17**, 84–85 (2003).
40. Fang, M., Chen, J. H., Xu, X. L., Yang, P. H. & Hildebrand, H. F. Antibacterial activities of inorganic agents on six bacteria associated with oral infections by two susceptibility tests. *Int. J. Antimicrob. Agents* **27**, 513–517 (2006).
41. Jones, N., Ray, B., Ranjit, K. T. & Manna, A. C. Antibacterial activity of ZnO nanoparticle suspensions on a broad spectrum of microorganisms. *FEMS Microbiol. Lett.* **279**, 71–76 (2008).
42. Touati, D. Iron and oxidative stress in bacteria. *Arch. Biochem. Biophys.* **373**, 1–6 (2000).
43. Makhluf, S. *et al.* Antimicrobial activity of SnO2 nanoparticles against *Escherichia coli* and *Staphylococcus aureus* and conventional antibiotics. *Adv. Funct. Mater.* **15**, 1708–1715 (2005).
44. Mei, X. J., Wang, Z. W. & Zheng, X. Soluble microbial products in membrane bioreactors in the presence of ZnO nanoparticles. *J. Memb. Sci.* **451**, 169–176 (2014).
45. Zietsman, A. *et al.* Cancer in Namibia 2006–2009. *Namibian Cancer Registry* **2**, 2 (2009).

Acknowledgements

This research was supported by the German DAAD, the French CNRS, the National Research Foundation of South Africa, the University of South Africa, iThemba-LABS as well as the UNESCO UNISA ITLABS-Africa Chair in Nanosciences & Nanotechnologies (U2ACN2). Ms. Adele Teymouri is specially acknowledged for her sound advices & fruitful discussions on pigments. Likewise, we wish to acknowledge Dr. UGRO for assisting with the background of Figure 1a.

Author contributions

DH: Data collection, analysis & manuscript writing,RA: Data collection & analysis,SA: Data collection & analysis,LM: EDS analysis, & Data collection & AnalysisJS: Data Collection & AnalysisNS: Research project management, review from the anthropological perspectiveAG: Manuscript review& various inputsMM: project inception, data analysis, interpretation & manuscript writing.

Competing interests

The authors declare no competing interests.

Additional information

Correspondence and requests for materials should be addressed to D.H. or M.M.